A study of the Diesel spray dynamics using Eulerian-Eulerian Large Eddy Simulation

Lionel Martinez*,[a], Adlène Benkenida[a], Bénédicte Cuenot[b]

[a] *IFP, 1 et 4 avenue Bois Préau, 92852, Rueil Malmaison Cedex, France*
[b] *CERFACS, 4 avenue G. Coriolis , 31055, Toulouse Cedex 01, France*

Abstract

The Large Eddy Simulation (LES) of Diesel Spray using an Eulerian-Eulerian approach is conducted and discussed. A two-fluid model based on the Mesoscopic Eulerian Formalism (MEF) is presented with the inclusion of collision effects inspired from the kinetic theory. The main objective of this study is to evaluate the ability of LES for Diesel sprays and to analyse the dynamics of both the gas and the liquid phases. The validation of the model is obtained through comparison with an experiment of Diesel fuel sprays in dense air. Mean axial spray velocity and its rms fluctuations are analysed for different pressures in the chamber and a sensitivity study on boundary conditions is discussed. The spray dynamics is deeply analysed by comparison with experimental results from the literature on turbulent gaseous jets. The analyse is focused on self-similarity and a comparison between a free gaseous jet and a spray is suggested.

Key words:
Diesel spray, Large Eddy Simulation, (LES), Mesoscopic Eulerian Formalism (MEF), self-similarity

1. Introduction

Nowadays, a better understanding of the combustion instabilities and cyclic variabilities in Internal Combustion (IC) engine is essential for car manufacturers. The non-deterministic character of the turbulence is one of the phenomena leading to the cyclic variability. It corresponds to the microscopic events that can influence the instantaneous velocity field and the local mixture leading to different heat release, pollutant levels and engine work from cycle to cycle (Ozdor et al., 1994). Computational Fluid Dynamics (CFD) is a helpful tool for studying such issues. The RANS (Reynolds Averaged Navier-Stokes) approach (Launder and Spalding, 1972) is commonly used in CFD to perform 3D simulations (Drake and Haworth, 2007). However, although it is characterised by reasonable computational costs, it does not allow the study of cyclic variabilities: RANS calculation of a given engine operation point represents the statistical average of many cycles at this point. Large Eddy Simulation (LES) is better adapted for such studies, as one LES of a given engine operation point may be view as one realization of one engine cycle. Computing local and instantaneous filtered properties (Sagaut, 1998), LES has demonstrated its capabilities in many configurations (Selle et al., 2006; Schmitt et al., 2007) and in particular in multi-cycle simulation of IC engine (Richard et al., 2007; Vermorel et al., 2007).

Due to its potential to resolve large scale vortices and so to predict the interaction between drops and air (carrier phase), LES is also of great interest for spray simulations (Bellan, 2000). Indeed, the level of turbulence intensity generated by the spray as well as the local composition of the gas mixture including fuel vapour are of critical importance for the combustion and pollutants production in IC engines.

The present study is devoted to the analysis of the spray dynamics using two-fluid Large Eddy Simulation. The liquid phase is described using an Eulerian approach, preferred to the Lagrangian particle tracking method for its potential to model complex industrial two-phase flows with high particles load and high

computational efficiency on massively parallel computer. Few publications have been devoted to the Eulerian-Eulerian simulation of sprays is realistic Diesel injections (Iyer and Abraham, 1997, 1998, 2005; Truchot and Magnaudet, 2005). Furthermore all these works concern RANS simulation. Therefore, is it of interest to investigate how the Eulerian-Eulerian LES for Diesel sprays compares with existing experimental data.

The Mesoscopic Eulerian Formalism (MEF) (Fevrier et al., 2005) is used here for the liquid phase. The physics of the Diesel spray imposes to take into account particle-particle interactions which are difficult to model in an Eulerian approach. Here, based on the work of Boelle et al. (1995) inspired from the kinetic theory, binary bouncing collisions are accounted for. The validation of the model is obtained through comparison with the experimental data of Chaves et al. (2004). A sensitivity study on the inflow turbulent boundary condition is also discussed as it can highly impact the development of the spray.

The Diesel spray is a transient, fully turbulent, two-phase flow and is consequently difficult to study experimentally and theorically. Few detailed experimental data are available in realistic Diesel injection conditions. Consequently, it seems worthwhile to study, in addition, LES spray results by analogy with the turbulent gaseous jet. This analogy has been examined by different authors (Dent, 1971; Spalding, 1979; Kuo and Bracco, 1982; Wu et al., 1984) because, contrary to the turbulent statistics of the spray, those of the jet have been largely investigated. One interesting point in jet flow is the self-similarity which has been confirmed by experiments (Wygnansky and Fielder, 1969; Panchapakesan and Lumley, 1993; Hussein et al., 1994). For the spray, the self-similarity is used by different researchers as hypothesis in their spray models (Desantes et al., 2006, 2007; Martinez et al., 2009) even if the identification of self-similar regions is not strictly established. With our LES, we should be able to investigate by an analysis of the dynamics of both the gas and the liquid phases, the existence of self-similar region.

The paper is organised as follows. First, the governing equations for LES are presented for both the gas and the liquid phase. The modelling and closure

terms are also defined and discussed in the framework of Direct Injection. Then, the simulation of the configuration of Chaves et al. (2004) is presented and a comparison between experimental data and numerical results is done. A sensitivity study on the boundary conditions is additionally proposed in order to find out the important parameters influencing the development of the spray. Finally, an extensive analysis of the behaviour of the droplets and the entrained gas is suggested by means of the turbulent statistics and focusing on self-similarity.

2. Governing equations and modelling

Both gas and liquid phases are simulated using an Eulerian formulation (Eulerian-Eulerian approach) and are two-way coupled through the drag force. No mass nor heat transfer are considered because the simulations concern only the non vaporising spray. The Eulerian conservation equations for the liquid are based on the Mesoscopic Eulerian Formalism developed by Fevrier et al. (2005) and extended to dense sprays by the addition of collision effects.

2.1. Carrier phase

In a LES approach, only the large scale eddies are resolved whereas the small scale eddies are modelled. Differentiation between large and small scale structures is done by filtering, defined as a convolution product of any variable f with a spatial filter kernel G_{Δ_f} of characteristic length Δ_f . The filtered quantity is then written as :

$$\bar{f}(x) = \int f(x) G_{\Delta_f}(x' - x) dx' \tag{1}$$

The Favre average is commonly used and allows to avoid density fluctuations. The Favre filtered quantity $\widetilde{f}(x)$ is written as :

$$\bar{\rho}\widetilde{f}(x) = \int \rho f(x) G_{\Delta_f}(x' - x) dx' \tag{2}$$

where $\bar{\rho}$ is the filtered density. From now on and for the sake of simplicity the filtered density will be written ρ in the paper. The subscript $_g$ will refer to

the gas phase whereas $_l$ will refer to the liquid phase. Applying this filtering on the Navier-Stokes equations leads to the filtered equations of respectively mass, momentum and energy :

$$\frac{\partial}{\partial t}\rho_g + \frac{\partial}{\partial x_i}\rho_g \widetilde{U}_{g,i} = 0 \tag{3}$$

$$\frac{\partial}{\partial t}\rho_g \widetilde{U}_{g,i} + \frac{\partial}{\partial x_j}\rho_g \widetilde{U}_{g,i}\widetilde{U}_{g,j} = -\frac{\partial}{\partial x_i}\bar{P} + \frac{\partial}{\partial x_j}\bar{\tau}_{g,ij} - \bar{F}_{drag} - \frac{\partial}{\partial x_j}T_{g,ij} \tag{4}$$

$$\frac{\partial}{\partial t}\rho_g \widetilde{E}_g + \frac{\partial}{\partial x_j}(\rho_g \widetilde{E}_g + \bar{P})\widetilde{U}_{g,j} = \frac{\partial}{\partial x_j}\bar{\tau}_{g,ij}\widetilde{U}_{g,j} - \bar{F}_{drag}\widetilde{U}_{l,i} - \frac{\partial}{\partial x_j}\bar{q}_{g,j} - \frac{\partial}{\partial x_j}Q_{g,j} \tag{5}$$

where $\widetilde{U}_{g,i}$ is the filtered velocity, and $\widetilde{E}_g$ is the filtered total non chemical energy. $\bar{P}$ is the filtered pressure, $\bar{\tau}_{g,ij}$ the filtered viscous stress tensor and $T_{g,ij} = 2\rho_g \mu_t \sqrt{2\tilde{S}_{g,ij}\tilde{S}_{g,ij}}\tilde{S}_{g,ij}$ is the subgrid scale tensor or Reynolds tensor where $\tilde{S}_{g,ij}$ is the strain rate tensor of the carrier phase :

$$\tilde{S}_{g,ij} = \frac{1}{2}\left(\frac{\partial \widetilde{U_{g,i}}}{\partial x_j} + \frac{\partial \widetilde{U_{g,j}}}{\partial x_i}\right) \tag{6}$$

The subgrid or eddy viscosity μ_t is modelled via the dynamic Smagorinsky model of Germano et al. (1991). The filtered heat flux is denoted $\bar{q}_{g,j}$ while the term $Q_{g,j}$ is the subgrid scale heat flux. $\bar{F}_{drag}$ is the filtered drag force, detailed in Section 2.2.

The set of equations (3)-(5) is based on the assumption that there is no effect of liquid volume on the carrier phase behaviour. This hypothesis implies thin spray. Furthermore, another hypothesis is that there is no modification of the carrier phase Reynolds tensor $T_{g,ij}$ due to the interaction with the liquid phase.

2.2. Dispersed phase

The Eulerian conservation equations are presented here for non evaporating sprays and without atomisation nor coalescence. The collision are nevertheless taken into account (see Section 2.2.4).

2.2.1. Mesoscopic Eulerian formalism

The Mesocopic Eulerian Formalism of Fevrier et al. (2005) accounts for the Random Uncorrelated Motion (RUM) detailed below and was first developed for diluted two-phase flow.

In a cloud of particles, different velocities may be found at close locations, depending on the particle histories. The instantaneous velocity $V^{(k)}(t)$ of a particle k located at position $X^{(k)}(t)$ may be decomposed into a statistical instantaneous Eulerian component shared by all the particles (the correlated velocity $\check{u}_p(t)$ or Mesoscopic Eulerian Velocity) and a residual velocity component, specific to the particle (uncorrelated velocity (RUM) $\delta u_p^{(k)}(t)$):

$$V^{(k)}(t) = \check{U}_l\left(X^{(k)}(t), t\right) + \delta u_p^{(k)}(t) \tag{7}$$

The contribution of the RUM is described *via* a probability density function (pdf) conditioned on one realization of the carrier phase. The principle for the establishment of the Eulerian liquid transport equation is similar to the derivation of the Navier-Stokes equations by the kinetic theory (Chapman and Cowling, 1939). These equations are obtained by integration over the phase space of the Boltzmann-type equation of evolution of the pdf (Fevrier et al., 2005; Riber et al., 2006; Moreau, 2005).

Then the Favre filter is applied to the transport equations of droplets to obtain the Eulerian filtered equations used in LES. The Favre operator is similar to the one used for the gas, replacing the density ρ_g by the particle number density n_l:

$$\bar{n}_l\widehat{f}(x) \quad = \quad \int n_l f(x) G_{\Delta_f}(x'-x)dx' \tag{8}$$

where n_l is the number density.

Finally, the following conservation equations of number density and mass are obtained:

$$\frac{\partial}{\partial t}\bar{n}_l + \frac{\partial}{\partial x_i}\bar{n}_l\widehat{U}_{l,i} = 0 \quad (9)$$

$$\frac{\partial}{\partial t}\bar{\alpha}_l\rho_l + \frac{\partial}{\partial x_i}\bar{\alpha}_l\rho_l\widehat{U}_{l,i} = 0 \quad (10)$$

where the filtered liquid volume fraction is defined as $\bar{\alpha}_l = \bar{n}_l\pi d^3/6$, ρ_l is the mass density of the liquid (considered constant), $\widehat{U}_l$ is the filtered correlated velocity and d is the particle diameter. The filtered momentum equation is:

$$\frac{\partial}{\partial t}\bar{\alpha}_l\rho_l\widehat{U}_{l,i} + \frac{\partial}{\partial x_j}\bar{\alpha}_l\rho_l\widehat{U}_{l,i}\widehat{U}_{l,j} = \bar{F}_{drag} - \frac{\partial}{\partial x_j}T_{l,ij} + \frac{\partial}{\partial x_j}\widehat{\delta\Sigma_{l,ij}} \quad (11)$$

The drag force is written as:

$$\bar{F}_{drag} = \frac{\bar{\alpha}_l\rho_l}{\tau_p}\left(\widetilde{U}_{g,i} - \widehat{U}_{l,i}\right) \quad (12)$$

where τ_p is the Stokes characteristic time defined from the drag coefficient C_D (Schiller and Nauman, 1935) and the particle Reynolds number R_e:

$$\tau_p = \frac{4}{3}\frac{\rho_l}{\rho_g}\frac{d}{C_D|V_r|} \text{ with } C_D = \frac{24}{R_e}\left(1 + 0.15R_e^{0.687}\right) \text{ and } R_e = \frac{\rho_g d|V_r|}{\mu_g} \quad (13)$$

where μ_g is the fluid molecular dynamic viscosity, $|V_r| = |\widetilde{U}_g - \widehat{U}_l|$ is the relative velocity between gas and liquid. $T_{l,ij}$ is the particle subgrid stress tensor. The last term of the right hand side (rhs) of Eq. (11) is the flux of the filtered stress tensor $\widehat{\delta\Sigma_{l,ij}} = -\frac{2}{3}\bar{\alpha}_l\rho_l\widehat{\delta\theta}_l\delta_{ij} - \bar{\alpha}_l\rho_l\widehat{\delta R^*_{l,ij}}$. It is based on the deviatoric part of the Random Uncorrelated Velocity (RUV) tensor $\widehat{\delta R^*_{l,ij}}$ and the filtered Random Uncorrelated Energy (RUE) $\widehat{\delta\theta}_l$, defined as the half of the RUV tensor trace (Simonin et al., 2002) and (Kaufmann, 2004). The term $2/3\bar{\alpha}_l\rho_l\widehat{\delta\theta}_l = P_{RUV}$ is a dilatation term that plays a role similar to a pressure term. A transport equation may be written for RUE as:

$$\frac{\partial}{\partial t}\bar{\alpha}_l\rho_l\widehat{\delta\theta}_l + \frac{\partial}{\partial x_i}\bar{\alpha}_l\rho_l\widehat{\delta\theta}_l\widehat{U}_{l,i} = -2\frac{\bar{\alpha}_l\rho_l}{\tau_p}\widehat{\delta\theta}_l - \frac{\partial}{\partial x_j}\bar{\alpha}_l\rho_l\widehat{\delta K_{l,iij}} + \widehat{\delta\Sigma_{l,ij}}\frac{\partial}{\partial x_j}\widehat{U}_{l,i} + \Pi_{\delta\theta_l} \quad (14)$$

The first term of the rhs is the RUE loss by drag force. It means that particles which are submitted to the carrier phase influence tend to have the same velocity. The second term is a diffusion term while the third term is a production term by shear and compression. The fourth term is a production term by subgrid scales.

2.2.2. Closure models for Random Uncorrelated Motion

The RUV tensor $\widehat{\delta R^*_{l,ij}}$ and the term $\widehat{\delta K_{l,ij}}$ of Eq. (14) are modelled, respectively, by a viscous assumption and by a diffusion term similar to Fick's law (Kaufmann, 2004):

$$\widehat{\delta R^*_{l,ij}} = -2\widehat{\nu_{RUV}}\left(\hat{S}_{l,ij} - \frac{\hat{S}_{l,mm}\delta_{ij}}{3}\right) = -2\widehat{\nu_{RUV}}\hat{S}^*_{l,ij} \tag{15}$$

$$\widehat{\delta K_{l,iij}} = -\widehat{\kappa}_{RUV}\frac{\partial\widehat{\delta\theta_l}}{\partial x_j} \tag{16}$$

where $\hat{S}_{p,ij}$ is the strain-rate tensor defined as :

$$S_{l,ij} = \frac{1}{2}\left(\frac{\partial\widehat{U_{l,i}}}{\partial x_j} + \frac{\partial\widehat{U_{l,j}}}{\partial x_i}\right) \tag{17}$$

The viscosity $\widehat{\nu}_{RUV}$ and the diffusion coefficient $\widehat{\kappa}_{RUV}$ are modelled as:

$$\widehat{\nu}_{RUV} = \frac{\tau_p}{3}\widehat{\delta\theta_l} \tag{18}$$

$$\widehat{\kappa}_{RUV} = \frac{10}{27}\tau_p\widehat{\delta\theta_l} \tag{19}$$

These models have been validated in an *a priori* study based on gas particle homogeneous isotropic turbulence (Moreau, 2005).

2.2.3. Closure models for subgrid terms

Models proposed by Moreau (2005) and Riber et al. (2005) for subgrid terms are used for the computations. Because of the high compressibility of the dispersed liquid phase, the subgrid scale (SGS) tensor $T_{l,ij}$ is decomposed into two parts. The diagonal part is equivalent to a subgrid pressure P_{SGS} proportional

to the subgrid energy and the non-diagonal part equivalent to a subgrid viscous tensor $T^*_{l,ij}$:

$$T_{l,ij} = \underbrace{C_l 2\Delta_f^2 \bar{\alpha}_l \rho_l |\hat{S}_l|^2 \delta_{ij}}_{P_{SGS}} - \underbrace{C_s 2\Delta_f^2 \bar{\alpha}_l \rho_l |\hat{S}_l| \left(\hat{S}_{l,ij} - \frac{\delta_{ij}}{3} \hat{S}_{l,kk} \right)}_{T^*_{l,ij}} \quad (20)$$

with $|\hat{S}_l|^2 = 2\hat{S}_{l,ij}\hat{S}_{l,ij}$. These models have been validated *a priori* in gas particle homogeneous isotropic turbulence (Moreau, 2005) and the values $C_s = 0.02$ et $C_l = 0.012$ were found.

The RUE production by subgrid scales $\Pi_{\delta\theta_l}$ is obtained by assuming that the correlated energy dissipated by subgrid effect is totally converted into RUE and the drag effect is negligible Riber et al. (2006). This leads to the relation:

$$\Pi_{\delta\theta_l} \approx -T_{l,ij} \frac{\partial}{\partial x_j} \widehat{U_{l,i}} \quad (21)$$

2.2.4. Extension to dense sprays : collision effects

The closure for RUV terms are linked to the drag force. For non-colliding particles, the increase or decrease of uncorrelated motion is due to the interaction with the carrier phase. For instance, small size droplets approach the same velocity which is the velocity of the carrier phase. Then, the uncorrelated energy decreases. On the other hand, the uncorrelated motion can be produced by shear or compression. Under the influence of vortices, the behaviour of droplets depends on their size and then their trajectories can be different. This could produce uncorrelated motion.

Thus, the drag force is the predominant effect which is taken into account for the evolution of the RUM. This hypothesis is only valid when the relaxation time is the minimum relevant time scale. In the dense zone of the spray, the collision time can be smaller than the relaxation time. It means that the droplet does not have the time to be influenced by the carrier phase. Therefore one has to adapt the equation and hypothesis for the closure of the RUV terms in order to take into account the collision effects. For this purpose an analogy is

proposed between the RUE and the granular temperature often used in fluidized beds simulation. One hypothesis is that the collisions are only binary, slightly inelastic and purely bouncing. Therefore coalescence is omitted and the model should be improved for this case. This point is highly questionable in non evaporating sprays. The coalescence can appear far from the nozzle exit and can lead to an increase in the mean diameter. In evaporating spray, in real IC engines conditions, the characteristic time of evaporation is so small, compared to a flow through time, that coalescence is negligible.

The model used here has been validated on simple shear dense suspensions (Boelle et al., 1995). The principles and developments of the model is reviewed by Peirano and Leckner (1998). The collision time (Chapman and Cowling, 1939) reads:

$$\tau_c = \frac{d}{24 g_0 \bar{\alpha}_l} \sqrt{\frac{3\pi}{2\widehat{\delta\theta}_l}} \quad \text{with} \quad g_0 = \left(1 - \frac{\bar{\alpha}_l}{\alpha_m}\right)^{-2.5\alpha_m} \tag{22}$$

where g_0 is the radial distribution function (Lun and Savage, 1986) with $\alpha_m = 0.6$.

The collision effects change the modelling of the RUV viscosity and diffusion defined in Eq. (18) and Eq. (19) to introduce the collisional time. The subscript c is used for the corrected kinematic terms ν_{RUV_c} and κ_{RUV_c}

$$\widehat{\nu}_{RUV_c} = \frac{\tau_p}{3}\widehat{\delta\theta}_l \left(1 + \bar{\alpha}_l g_0 \frac{2}{5}(1+e)(3e-1)\right) \frac{1}{\left(1 + \frac{\tau_p}{\tau_c}\frac{(1+e)(3-e)}{10}\right)} \tag{23}$$

$$\widehat{\kappa}_{RUV_c} = \frac{2}{3}\widehat{\delta\theta}_l \frac{\left(1 + \bar{\alpha}_l g_0 \frac{3}{5}(1+e)^2(2e-1)\right)}{\left(\frac{9}{5\tau_p} + \frac{(19-33e)(1+e)}{100\tau_c}\right)} \tag{24}$$

where e is the restitution coefficient which is set to a fixed arbitrary value $e = 0.9$. The influence of e on the stress has already been studied by different authors (Campbell, 1989; Hopkins and Louge, 1991). Additional terms, linked

to collision effects also appear like the collisional stress tensor $\widehat{\delta\Sigma^{coll}_{l,ij}}$ and a collisional diffusion term $\widehat{\delta K^{coll}_{l,iij}}$ which are modelled similarly to the kinematic terms $\widehat{\delta\Sigma_{l,ij}}$ and $\widehat{\delta K_{l,iij}}$, *i.e.* respectively by a Boussinesq assumption and by a diffusion term similar to Fick's law:

$$\widehat{\delta\Sigma^{coll}_{l,ij}} = -\left(\widehat{P}_{coll} - \widehat{\xi}_c \hat{S}_{l,kk}/3\right)\delta_{ij} + 2\bar{\alpha}_l\rho_l\widehat{\nu_{coll}}\hat{S}^*_{l,ij} \tag{25}$$

$$\widehat{\delta K^{coll}_{l,iij}} = -\widehat{\kappa}_{coll}\frac{\partial\widehat{\delta\theta}_l}{\partial x_j} \tag{26}$$

where $\widehat{\nu}_{coll}$ is the collisional viscosity (Boelle et al., 1995):

$$\widehat{\nu}_{coll} = \left(\frac{4}{5}\bar{\alpha}_l g_0(1+e)\left(\widehat{\nu}_{RUV_c} + d\sqrt{\frac{2\widehat{\delta\theta}_l}{3\pi}}\right)\right) \tag{27}$$

$\widehat{\kappa}_{coll}$ is the collisional diffusivity:

$$\widehat{\kappa}_{coll} = \bar{\alpha}_l g_0(1+e)\left(\frac{6}{5}\kappa_{RUV_c} + \frac{4}{3}d\sqrt{\frac{2\widehat{\delta\theta}_l}{3\pi}}\right) \tag{28}$$

$\widehat{P}_{coll}$ is the collisional pressure:

$$\widehat{P}_{coll} = \frac{4}{3}\bar{\alpha}_l^2\rho_l g_0(1+e)\widehat{\delta\theta_l} \tag{29}$$

$\widehat{\xi}_c$ is the bulk viscosity:

$$\widehat{\xi}_c = \frac{4}{3}\bar{\alpha}_l^2\rho_l g_0(1+e)d\sqrt{\frac{2\widehat{\delta\theta}_l}{3\pi}} \tag{30}$$

The new model for stress and diffusive tensors, taking into account collision effects are:

$$\delta\Sigma^{tot}_{l,ij} = -\left(\widehat{P}_{RUV} + \widehat{P}_{coll} - \widehat{\xi}_c\hat{S}_{l,kk}/3\right)\delta_{i,j} + 2\bar{\alpha}_l\rho_l\left(\widehat{\nu}_{RUV_c} + \widehat{\nu}_{coll}\right)\hat{S}^*_{l,ij} \tag{31}$$

and

$$\widehat{\delta K^{tot}_{l,iij}} = -\left(\widehat{\kappa}_{RUV_c} + \widehat{\kappa}_{coll}\right)\frac{\partial\widehat{\delta\theta}_l}{\partial x_j} \tag{32}$$

Thus Eq. (11) and Eq. (14) become respectively:

$$\begin{aligned}\frac{\partial}{\partial t}\bar{\alpha}_l\rho_l\widehat{U}_{l,i}+\frac{\partial}{\partial x_j}\bar{\alpha}_l\rho_l\widehat{U}_{l,i}\widehat{U}_{l,j} &= \frac{\bar{\alpha}_l\rho_l}{\tau_p}\left(\widehat{U}_{g,i}-\widehat{U}_{l,i}\right)-\frac{\partial}{\partial x_j}T^*_{l,ij}-\frac{\partial}{\partial x_i}P_{SGS}\\ &-\frac{\partial}{\partial x_i}\widehat{P}_{RUV}-\frac{\partial}{\partial x_i}\widehat{P}_{coll}+\frac{\partial}{\partial x_i}\left(\widehat{\xi}_c\frac{\partial U_{l,k}}{\partial x_k}\right)\\ &+\frac{\partial}{\partial x_j}2\bar{\alpha}_l\rho_l\left(\widehat{\nu}_{RUV_c}+\widehat{\nu}_{coll}\right)S^*_{l,ij} \qquad (33)\end{aligned}$$

$$\begin{aligned}\frac{\partial}{\partial t}\bar{\alpha}_l\rho_l\widehat{\delta\theta_l}+\frac{\partial}{\partial x_i}\bar{\alpha}_l\rho_l\widehat{\delta\theta_l}\widehat{U}_{l,i} &= -2\frac{\bar{\alpha}_l\rho_l}{\tau_p}\widehat{\delta\theta_l}-\bar{\alpha}_l\rho_l\frac{1-e^2}{3\tau_c}\widehat{\delta\theta_l}\\ &-\frac{\partial}{\partial x_j}\bar{\alpha}_l\rho_l\widehat{\delta K^{tot}_{l,iij}}+\widehat{\delta\Sigma^{tot}_{l,ij}}\frac{\partial}{\partial x_j}\widehat{U}_{l,i}\\ &+\Pi_{\delta\theta_l} \qquad (34)\end{aligned}$$

This model can be seen as an extension of the diluted model. When the liquid volume fraction tends to zero, the collisional time tends to infinity and the collisional terms (Eq.(27, 28, 29, 30) naturally tend to zero. Furthermore the kinematic terms from Eq.(23,24) tend to their value for the diluted case.

2.2.5. Characteristic time scales for sprays and Stokes number

The ratio of the relaxation time (Eq. 13) and the collision time (Eq. 22) allows to evaluate the relative impact of the drag force and collisions. The Stokes number introduces an additional time scale, characteristic of the carrier phase, taken here as the characteristic time τ^t of the most energetic structures in a gas jet. The expansion of the jet along its axis is proportional to the distance from the jet exit X. Moreover, the axial velocity on the jet axis decreases like $1/X$. Then the turbulent time scale τ^t should be proportional to:

$$\tau^t \propto \frac{X^2}{U_{exit}.D} \qquad (35)$$

where U_{exit} is the spray velocity at the nozzle exit and D is the injector diameter. The Stokes number now reads :

$$St = \frac{\tau_p}{\tau^t} \quad \propto \quad \frac{\tau_p U_{exit}.D}{X^2} \tag{36}$$

An interesting point is that, the Stokes number decreases along the spray axis meaning that the droplets will be more influenced by the turbulence downstream of the jet.

3. Numerical Simulation

3.1. LES solver

The AVBP code, jointly developed and owned by IFP and CERFACS is used for the simulations. It solves the compressible Navier-Stokes equations for reactive two phase flows (Moureau, 2004) with low dissipation schemes adapted to LES (third order in space and time Taylor-Galerkin scheme TTGC (Colin and Rudgyard, 2000)). The abilities of AVBP in reactive two-phase flows have been investigated in gas turbine configuration (Boileau et al., 2008) and in multi-cycle IC engine simulation (Richard et al., 2007; Vermorel et al., 2007).

3.2. Experimental set-up

The experiment of Chaves et al. (2004) is investigated in this study. It corresponds to a Diesel-like liquid injection without cavitation at a moderate pressure ($\Delta P = 10MPa$) into a quiescent dense air ($3MPa$). The injector diameter is $D = 200\mu m$. The measurements are done when the injection reaches a quasi-steady state. The Bernoulli velocity is $154.7m/s$ for this case. The mean and fluctuating (rms) axial velocity profiles are provided at 10D and 100D from the nozzle exit.

3.3. Parameters of the simulation and boundary conditions

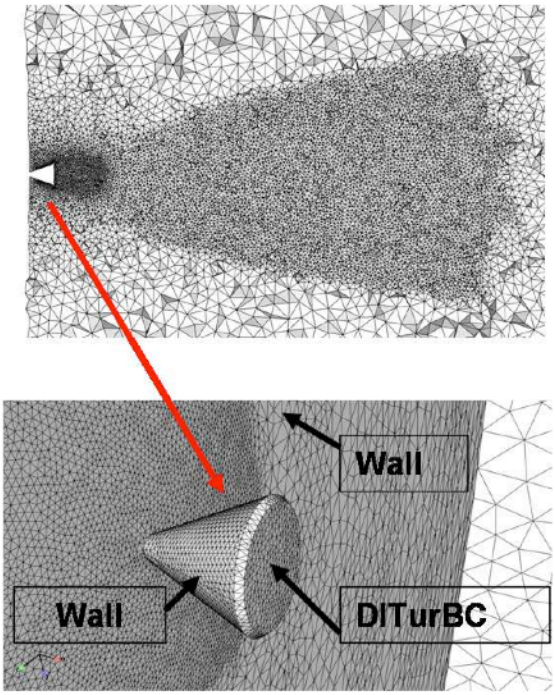

Figure 1: Cross section of the mesh and view of the cone dedicated to the DITurBC.

The tetrahedral 3D mesh (See Fig. 1) is composed of 350000 nodes, with a minimum edge length of $80\mu m$. The numerical parameters of the calculation are presented in Table (1).

Scheme :	Two-step Taylor-Galerkin TTGC* *(Colin and Rudgyard, 2000)
CFL :	$0,7$
Time step :	$5.810^{-8}s$
Physical time :	$2.5ms$
CPU time (32 proc. Opteron) :	$35h$

Table 1: Numerical parameters of the LES calculations.

The spray is formed by an atomisation process resulting from complex in-

terface phenomena that can not be reproduced with the present model and are not well understood. Therefore the droplets are directly introduced in the domain, following a procedure described in (Martinez et al., 2009) and called Downstream Inflow Turbulent Boundary Conditions (DITurBC).

The strategy consists of initiating the 3D simulation at 10D downstream from the nozzle exit. The mean radial profiles of axial velocity, liquid volume fraction and droplet diameters are supposed to be gaussian. The characteristics of the spray at the nozzle exit are calculated using data on nozzle geometry and the turbulent and the cavitating flow inside the nozzle. Then, additional conservation equations of mass and momentum between the nozzle exit and the boundary conditions are used to determine the mean profiles. Gas is also injected to represent the entrainment at the nozzle exit. The gas velocity is supposed to be equal to the liquid velocity. The application of a boundary condition at $10D$ downstream from the nozzle exit is made possible by the addition, in the geometry, of a solid cone that shifts the inlet boundary condition. The DITurBC model has been validated by comparison with the experiment of Chaves et al. (2004), affording to recover the profiles at 10D. The parameters of the boundary conditions are presented in Table (2) for what will be referred as the reference case.

Max. drop velocity:	$154m/s$
Max. gas velocity:	$154m/s$
Mean drop velocity:	$135m/s$
Mean gas velocity:	$135m/s$
Max. liquid volume fraction:	0.2
Max. Droplet diameter:	$20\mu m$
Turbulence intensity:	20%

Table 2: Boundary conditions for the reference case.

The physical parameters are presented in Table (3).

Ratio of density ρ_g/ρ_l:	0.043
Pressure in the chamber:	$30MPa$
Injection Pressure:	$130MPa$
Temperature of the chamber:	$293K$

Table 3: Physical parameters of the simulation for the reference case.

3.4. Turbulent boundary conditions

In order to create a turbulent field with a given statistical profile, a non-dimensional homogeneous fluctuating velocity field is generated. This field is then rescaled and added to the mean velocity profile on the DITurBC for both liquid and gas phases. The method is based on the work of Kraichnan (1970) and a similar method is used by Smirnov et al. (2001).

The divergence free, statistically stationary, homogeneous, isotropic, multivariate-normal velocity field, for N modes, is of the form:

$$v_i(x,t) = \sqrt{\frac{2}{N}} \sum_{n=1}^{N} \left[p_i^{(n)} \cos\left(k_e \lambda^{(n)} x_j + \omega^{(n)}\right) + q_i^{(n)} \sin\left(k_e \lambda^{(n)} x_j + \omega^{(n)}\right) \right] \tag{37}$$

where $p_i^{(n)} = \epsilon_{ijm} \xi_j^{(n)} \lambda_m^{(n)}$ and $q_i^{(n)} = \epsilon_{ijm} \zeta_j^{(n)} \lambda_m^{(n)}$. Here ϵ_{ijm} is the permutation tensor used in the vector-product operation. The variables $\xi_j^{(n)}$, $\zeta_j^{(n)}$ and $\lambda_j^{(n)}$ are random quantities. $\xi_j^{(n)}$ and $\zeta_j^{(n)}$ are calculated from normal distribution $N(0,1)$, *i.e.* with a mean of 0 and a standard deviation of 1. $\lambda_j^{(n)}$ is calculated from a Gaussian distribution $G(0,1/2)$.

For an infinite number of modes, the energy spectrum is of the form:

$$E(k) = \frac{2}{3} 16 \sqrt{\frac{2}{\pi}} \left(\frac{k}{k_e}\right)^4 \exp(-2k^2/k_e^2) \tag{38}$$

with a maximum energy for $k = k_e$ and a correlation length of the order $L_e = 1/k_e$.

In the paper of Kraichnan (1970), $\omega^{(n)}$ is obtained from a Gaussian distribution with standard deviation ω_0 leading to a time correlation of the form

$\exp(-\omega_0^2 t^2/2)$. Here a different approach is used. Instead of generating a 2D inlet field varying with time, a 3D field, *i.e.* 2D inlet + direction perpendicular to the inlet, is generated. At each time t, the field corresponding to the 2D section located at $U_{conv}.t$ upstream from the inlet section (in the direction perpendicular to the inlet) is injected, where U_{conv} is the mean velocity in direction perpendicular to the inlet plane. One can view the turbulent velocity field as velocity fluctuations in a grid turbulence with mean velocity U_{conv}.

From the homogeneous isotropic turbulent velocity field, an inhomogeneous fluctuating target velocity U_i^T is created to reproduce the statistical mean velocity $< U_i >$, the Root-Mean-Square (RMS) fluctuations $\sqrt{< u_i^{'2} >}$ and the cross correlations $< u_i^{'} u_j^{'} >$, using the tensor a_{ij} (Klein et al., 2003):

$$U_i^T(x,t) \quad = \quad < U_i(x) > + a_{ij}(x) v_j(x,t) \tag{39}$$

This allows to obtain an anisotropic field, more relevant for a jet simulation.

The RMS fluctuations u_{rms}, v_{rms}, w_{rms} are set to fit the turbulence intensity of a gas jet in the self-similarity area according to Hussein et al. (1994),

i.e. $(u_{rms}/ < U >)_{axis} = 0.25$, $(v_{rms}/ < U >)_{axis} = 0.20$ and $(w_{rms}/ < U >)_{axis} = 0.20$. For the simulation of the experiment of Chaves et al. (2004), in order not to exceed the Bernoulli velocity and to be in accordance with the experimental results at $10D$, the axial velocity fluctuations are set to $(u_{rms}/ < U >)_{axis} = 0.2$. A questionable point here is how to set the level of correlation between the gas and the liquid fluctuations. For the sake of simplicity and in a first approach, no correlation is supposed. This point will be discussed in section 4.4.

The amplitude of the velocity fluctuations are supposed equal for the gas and the liquid phase.

4. Results and analysis of the spray behaviour

The aim of this section is to evaluate the quality of the simulation by comparison with the experimental results of Chaves et al. (2004). The decrease of the

mean axial droplet velocity as well as its mean and RMS radial profiles at 100D are studied. A sensitivity study on some chosen boundary conditions parameters is proposed. In particular, the influence of the drag force, the turbulence intensity and the density of the air are addressed.

4.1. Effect of drag

The effect of drag is studied by changing either the maximum diameter of the droplets at injection or the inlet gas velocity at the boundary conditions. These effects are illustrated on Fig. (2).

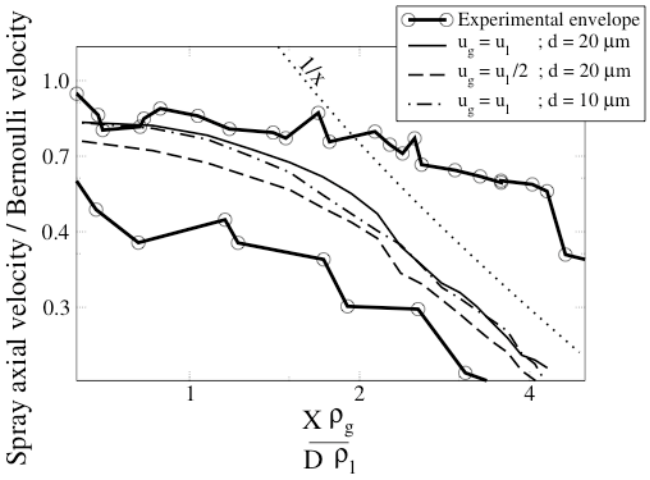

Figure 2: Decrease of mean axial velocity and effects of the inlet gas velocity.

For the reference case ($u_g = u_l$ and $d = 20\mu m$), the decrease of the mean axial velocity is within the experimental envelope or extrema. At a normalised distance of $(X/D)(\rho_g/\rho_l) = 2.5$ ($X/D \approx 60$), the mean axial velocity decreases like $1/X$ which corresponds to the decrease in a free jet of gas. This behaviour is the same with a maximum droplet diameter of $10\mu m$ and with a gas velocity equal to half the injected liquid velocity. The simulation is then insensitive to the droplet diameter and the gas velocity at injection.

The radial profiles are depicted on Fig. (3).

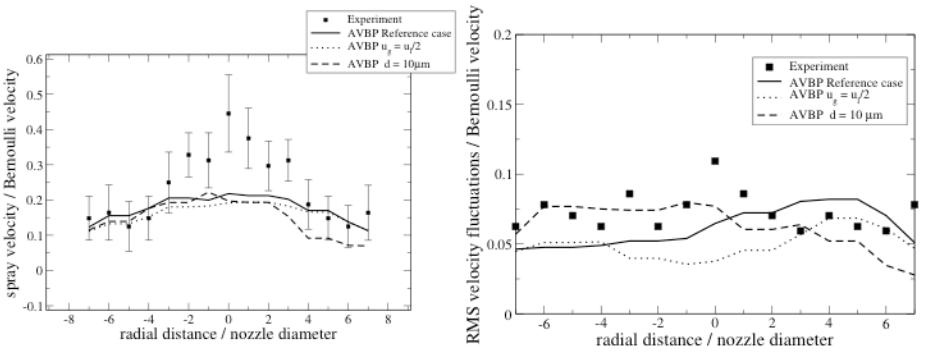

(a) Axial liquid mean velocity

(b) Axial liquid rms velocity

Figure 3: Radial distribution at $X/D = 100$ of mean and rms axial velocity. Comparison on the effect of the drag force.

The mean profiles are almost identical for the three cases. The mean axial velocity is under estimated by the simulation compared to the experimental results, especially near the spray axis. At the periphery the comparison is very good. The disagreement is probably due to very large droplets which are not included in our simulation but which could be present in the experiment because they have not been atomised. Due to their inertia, these droplets conserve high velocities and are concentrated near the spray axis. In the experiment of Chaves et al. (2004), the injection pressure is not realistic compared to the injection pressure in real Diesel engine that reach $200MPa$ and is maybe not high enough to produce small droplets. Then, the effect of large droplets may be expected less important in real engine conditions.

The RMS values show a good agreement with the experiment for the entire radial profiles excepted at the center. The reason is probably the same as described for the mean velocity.

In order to better understand these results, the energy exchange term appearing in Eq. (5) is averaged by the spray volume, normalised by its maximum and plotted versus time in Fig. (4) together with the evolution of the spray

volume.

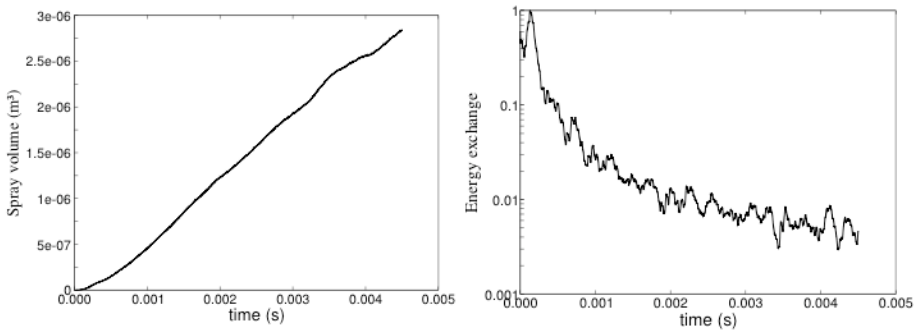

(a) Spray volume

(b) Energy exchange

Figure 4: Evolution of spray volume and energy exchange between phases with time.

The exchange of energy is higher at the beginning of the injection when the air begins to be entrained. Then, the exchange term decreases during the simulation proving an equilibrium between the liquid and the gas. This equilibrium is reached rapidly, as at $t = 2ms$ the exchange term is about 1% of its maximum. The equilibrim between liquid and gas was also noticed experimentally by Doudou (2005) in the central part of the spray.

4.2. Effect of the turbulence intensity

Contrary to drag force which seems to have a small influence on the spray development, the turbulence intensity is of first order as it controls the spray opening.

Fig. (5) shows an iso-surface of the gas vorticity magnitude and an iso-surface of the liquid volume fraction for different levels of turbulent intensity. With an intensity of $u_{rms}/ < U >= 1\%$, the spray presents small vortices,

i.e. small structures on the vorticity field, compared to the case of $u_{rms}/ < U >= 20\%$. The development of the turbulent structures is enhanced by the level of intensity. Furthermore the large scales vortices transport droplets to

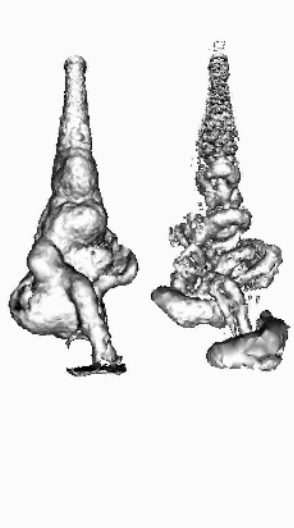

(a) reference case: $u_{rms}/ < U >= 20\%$

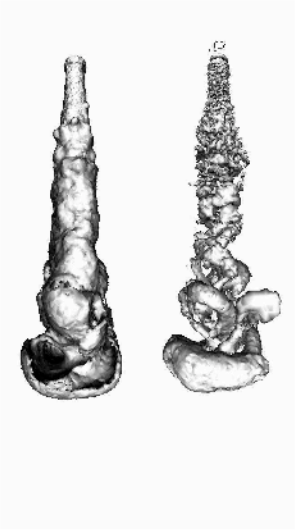

(b) $u_{rms}/ < U >= 10\%$

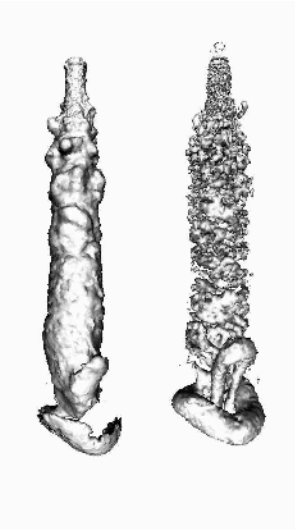

(c) $u_{rms}/ < U >= 1\%$

Figure 5: Instantaneous iso-surface of the liquid volume fraction (left) and the gas vorticity magnitude (right) for different levels of turbulence at $t = 2ms$.

the periphery of the spray and contribute to the spray opening as can be seen on the iso-surface of liquid volume fraction.

By conservation of the axial momentum flux, the spray opening is directly linked to the decrease of the axial velocity (See Fig. (6)). As a consequence, the

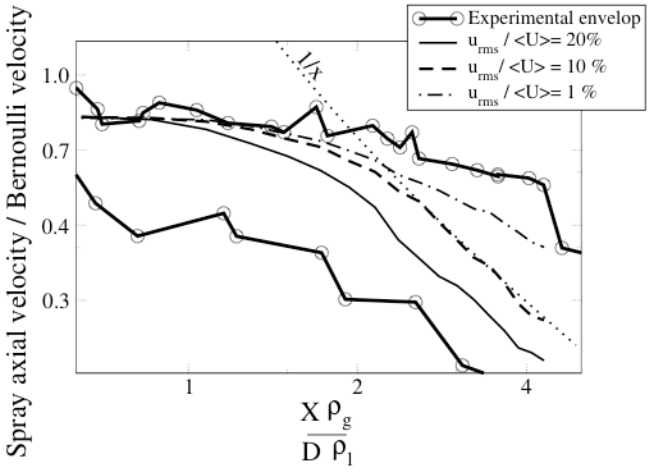

Figure 6: Decrease of mean axial velocity and effects of the level of turbulence.

decrease of velocity is less important in the case of low turbulence. Nevertheless, the profiles remain within the experimental extrema. In the case of $u_{rms}/ < U >= 1\%$, the decrease is not proportional to $1/x$ and thus the spray has not reached the behaviour of a free jet.

Surprisingly, the radial profiles on Fig. (7) are more in accordance with the experiment for the case of low turbulence which disagrees with the results on the spray angle. The main reason is probably again the presence of large droplets which have not been atomised have conserved a high velocity in the experiment.

4.3. Effect of the chamber pressure

The impact of the chamber pressure and consequently of the air density is studied. It has been observed many times that the decrease of the chamber pressure leads to a decrease of the spray angle and consequently to an increase of the penetration.

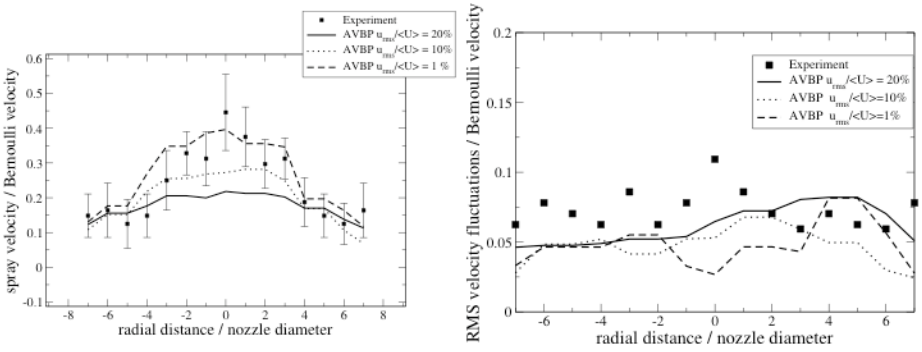

(a) Axial liquid mean velocity

(b) Axial liquid rms velocity

Figure 7: Radial distribution at $X/D = 100$ of mean and rms axial velocity. Comparison on the effect of the level of turbulence.

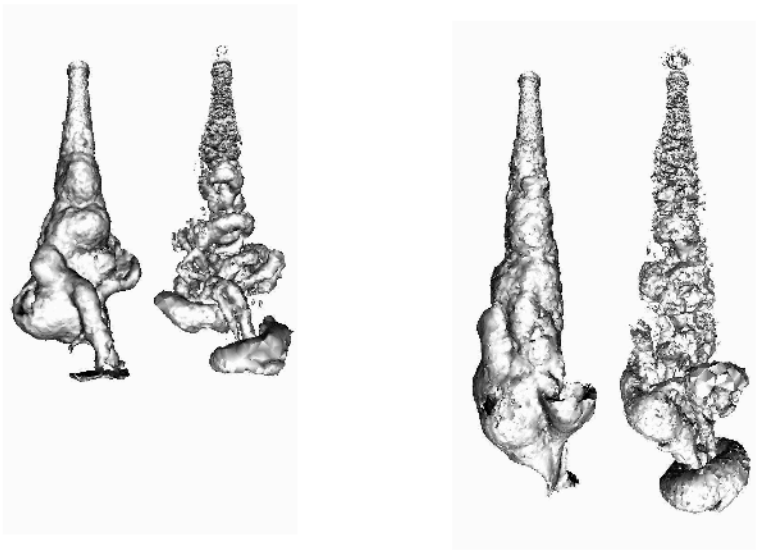

(a) reference case: $P = 3MPa$

(b) $P = 1MPa$

Figure 8: Instantaneous iso-surface of the liquid volume fraction (left) and the gas vorticity magnitude (right) for different back pressures at $t = 2ms$.

Fig. (8) shows that the calculations are able to capture these well-known phenomena. The decrease of the axial velocity along the spray axis is presented on Fig. (9).

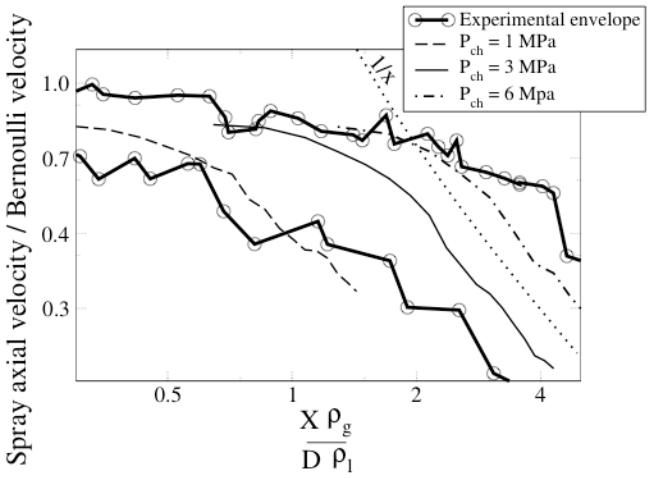

Figure 9: Decrease of mean axial velocity and effects of the boundary condition parameters.

For all the pressures, the liquid velocity descreases like $1/x$. According to Chaves et al. (2004), even with a change of the density, the profiles should remain in the experimental envelope. This is the case with the pressure of $P = 6MPa$. For the pressure of $P = 1MPa$, the decrease is slightly higher than the experimental measurements but the tendency is well predicted.

4.4. Self-similarity

The Diesel spray is a transient, fully turbulent, two-phase flow and is consequently difficult to study experimentally and theorically. Few detailed experimental data are available in realistic Diesel injection conditions. Consequently, it seems worthwhile to study, in addition, LES spray results by analogy with the turbulent gaseous jet. Spalding (1979) was one of the first to consider the Diesel spray as a gaseous turbulent jet. Ouellette and Hill (2000) have shown that, by comparison between turbulent gas jets and sprays with the same momentum injection rate and chamber pressure, penetration and mixing rates are

closely similar when the spray droplets diameters are small. This result was used by Bruneaux (2002) to study the mixture in Diesel like injection using visualizations in a gaseous fuel jet.

Many authors (Arcoumanis et al., 1989; Naber and Siebers, 1996) have noticed experimental similarities between them or have this property as an assumption in their spray models (Desantes et al., 2006, 2007).

Here, the sensitivity study presented in Section 4.1 shows that, for the reference case, the decrease of velocity is proportional to $1/x$ at about $60D$ from the nozzle exit, behaving therefore like a free gas jet. This results was also found by Payri et al. (2008) for higher injection pressures.

To go further in the comparison between a gaseous jet and spray self-similarity is studied for both gas and liquid phases. To go further, an analogy of behaviour can be deduced by looking at the turbulence intensity. By definition, in a gas jet, self-similarity is reached when the turbulence intensity stays constant along the spray axis. The turbulence intensity along the axis and for the three components are depicted on Fig. (10) for the gas phase and the liquid phase. The evolution of the ratio between the turbulent kinetic energy k and

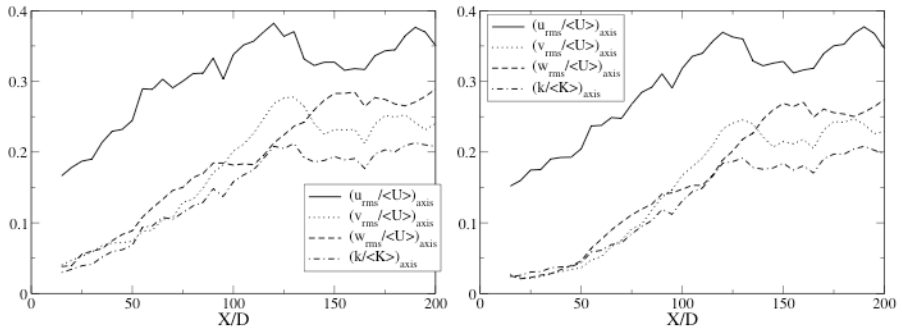

(a) Gas

(b) Liquid

Figure 10: Evolution of the turbulence intensity along axis for liquid and gas phase.

the mean kinetic energy $< K >$ is also presented. The main point is that from

$X/D = 125$, the turbulence intensity in the axial direction $(u_{rms}/ < U >)_{axis}$ is approximately constant for the gas. The ratio of energy is also approximately constant. The other components reach self-similarity at $X/D = 125$ for v_{rms} or $X/D = 150$ for w_{rms}. For the turbulent energy the similarity is reached at $X/D = 125$. The same conclusions hold for the liquid phase as both figures look very much the same. The fact that self-similarity is reached sooner for the axial fluctuation was also observed by Wygnansky and Fielder (1969) for a gaseous jet. Their experimental results give:

$$(u_{rms}/ < U >)_{axis} \approx 0.29 \text{ to } 0.27 \text{ for } X/D = 40 \text{ to } 96 \quad (40)$$

$$(v_{rms}/ < U >)_{axis} \approx 0.24 \text{ to } 0.25 \text{ for } X/D = 75 \text{ to } 96 \quad (41)$$

$$(w_{rms}/ < U >)_{axis} \approx 0.24 \text{ to } 0.25 \text{ for } X/D = 75 \text{ to } 96 \quad (42)$$

The present simulation results concerning the gas and liquid fluctuations are comparable with this experiment. Nevertheless, for the simulated spray, self-similarity is reached later and the axial fluctuations are higher.

One can also observe that the levels are slightly lower for the liquid than for the gas. An explanation is that the fluctuations for the liquid phase report only the mean correlated fluctuating motion. The mean uncorrelated part should be added to obtain the total fluctuation. The ratio between the mean uncorrelated part and the total turbulent kinetic energy is discussed in Section 4.6.

Experimentally, Doudou (2005) also found self-similarity for the radial distribution and for the turbulence intensity. The radial distributions of the mean liquid velocity normalized by the mean liquid velocity on the axis are presented on Fig.(11) for different axial distances. $y_{0.5}$ is the radial position where the velocity is equal to half the velocity on the spray axis. The first comment is that the normalized profiles are independent of the axial distance. This confirms the self-similarity. Furthermore, the results fit very well with the experimental results of Hussein et al. (1994) obtained in a free gas jet, arguing again in favor of same behaviour of a spray and free gas jet. The radial distributions for the

gas phase are not presented here because there are similar to those of the liquid phase.

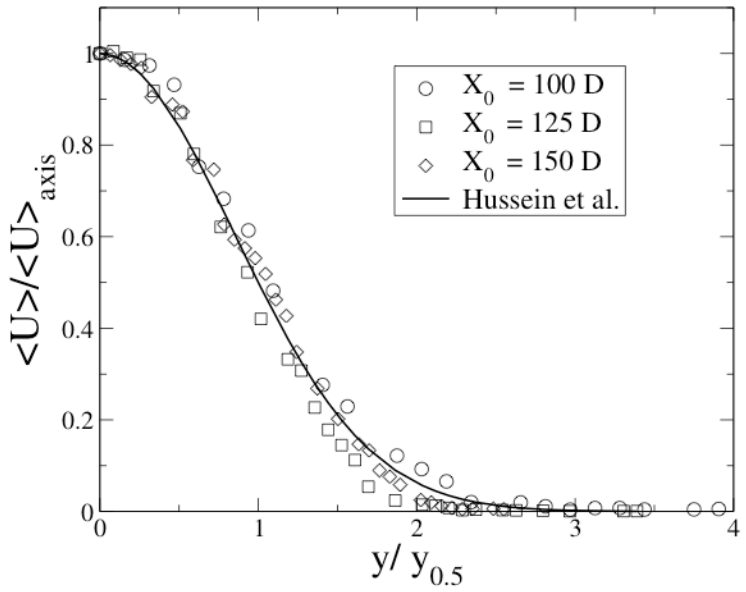

Figure 11: Self-similarity of the mean liquid axial velocity. Comparison with the experiment of Hussein et al. (1994).

The cross correlation coefficient C_{uv} defined as:

$$C_{uv} = -\frac{< u'v' >}{\sqrt{< u'^2 >}\sqrt{< v'^2 >}} \tag{43}$$

is shown in Fig. (12) for the gas phase and the liquid phase at $X/D = 100$. The results are compared to the results of Gibson (1963); Wygnansky and Fielder (1969); Panchapakesan and Lumley (1993) for a free gas jet. The first comment is that the behaviour for the gas and the liquid is the same as the experiment. Coefficients are increasing with the distance from the spray axis and seem to converge from $y/y_{0.5} = 1$. The levels are also comparable with the experiment even if they are slightly higher in the spray simulation.

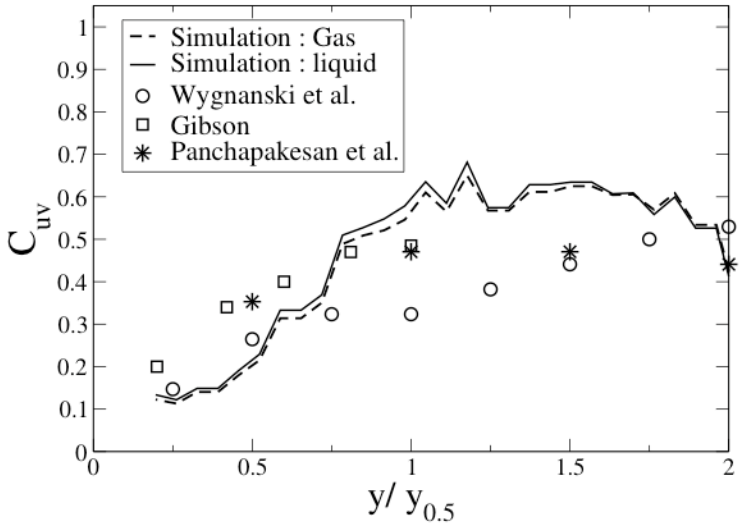

Figure 12: Coefficient of the cross correlation C_{uv} for the gas and liquid phase at X/D=100. Comparison with the experiments of Wygnansky and Fielder (1969), Gibson (1963) and Panchapakesan and Lumley (1993)

4.5. Droplet distribution

LES is able to capture the non homogeneity of the liquid volume fraction. Fig. (13) shows the local liquid volume fraction strongly perturbated by the turbulence. In evaporating sprays this will lead to locally high concentration of fuel and will impact the combustion and pollutant production.

4.6. Uncorrelated droplet velocity

In the mesoscopic formalism, according to Fevrier et al. (2005), the particle fluctuating velocity u_l' can be decomposed into a spatially correlated contribution $\widetilde{u_l'}$ and a random and spatially uncorrelated contribution $\delta u_l'$. Then, the total turbulent kinetic energy of the liquid phase is the sum of the mean kinetic energy of the fluctuating part of the correlated motion $\widetilde{q_p^2}$ and the mean random uncorrelated energy δq_p^2. Vance et al. (2006) have proposed a correlation that permits to evaluate the ratio $\delta q_p^2/\widetilde{q_p^2}$. Compared to the correlation of Fevrier et al. (2005), Vance's correlation has a greater range of applicability since it

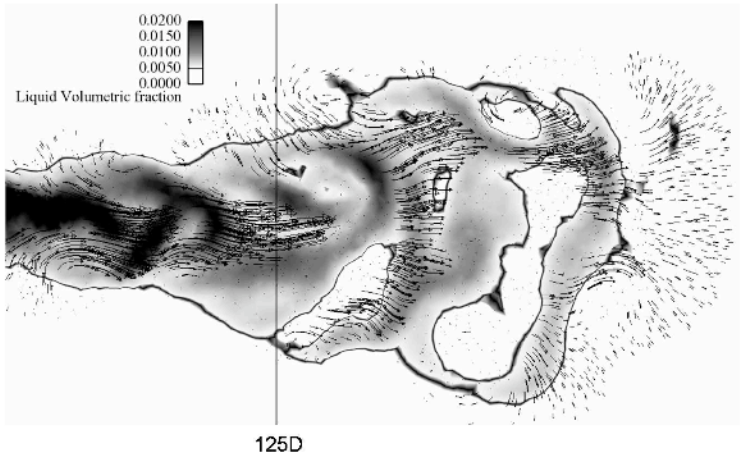

Figure 13: Cross section view. Instantaneous liquid volume fraction field and gas velocity vectors.

applies with and without collisions and is especially improved in the near-wall region which is far from equilibirum. The correlation formulates that the fraction of the velocity variance residing in the correlated motion is reasonably approximated by the square-root of the fluid-particle correlation coefficient:

$$\frac{< \widetilde{u'_{i,l}}^{\,2} >}{< u'^{\,2}_{i,l} >} \approx \sqrt{\frac{< u'_{i,g} u'_{i,l} >^2}{< u'^{\,2}_{i,g} >< u'^{\,2}_{i,l} >}} \tag{44}$$

where i is the i-*th* component of the velocity. This expression can be extended to an energy correlation by observing that $< u'_{i,l} >=< \delta u'_{i,l} > + < \widetilde{u'_{i,l}} >$. Then using, the inverse of Eq. (44), one gets:

$$\frac{< \delta u'^{\,2}_{i,l} >}{< \widetilde{u'_{i,l}}^{\,2} >} \approx \sqrt{\frac{< u'^{\,2}_{i,g} >< u'^{\,2}_{i,l} >}{< u'_{i,g} u'_{i,l} >^2}} - 1 \tag{45}$$

Using again Eq. (44) to express $< u'^{\,2}_{i,l} >$ and substituting in Eq. (45) gives :

$$\frac{< \delta u'^{\,2}_{i,l} >}{< \widetilde{u'_{i,l}}^{\,2} >} \approx \frac{< \widetilde{u'_{i,g}}^{\,2} >< u'^{\,2}_{i,l} >}{< u'_{i,g} u'_{i,l} >^2} - 1 \tag{46}$$

According to Fevrier et al. (2005), the fluid-particle correlation can be simplified using the correlated part of the liquid fluctuation:

$$< u'_{i,g} u'_{i,l} >^2 \approx < u'_{i,g} \widetilde{u'_{i,l}} >^2 \tag{47}$$

Then, one gets:

$$\frac{< \delta u'_{i,l}{}^2 >}{< \widetilde{u'_{i,l}}^2 >} \approx \underbrace{\frac{< \widetilde{u'_{i,g}}^2 >< u'_{i,l}{}^2 >}{< u'_{i,g} \widetilde{u'_{i,l}} >^2} - 1}_{Va_i} \tag{48}$$

Here, it is interesting to use the correlation in terms of energy:

$$\frac{\delta q_p^2}{\widetilde{q_p^2}} \approx \frac{\sum_{i=1}^{3} < \widetilde{u'_{i,l}}^2 > Va_i}{\sum_{i=1}^{3} < \widetilde{u'_{i,l}}^2 >} \tag{49}$$

This correlation is compared in Fig. (14) to the value of $\delta q_p^2 / \widetilde{q_p^2}$ obtained in the simulation, showing that uncorrelated energy is under-estimated before

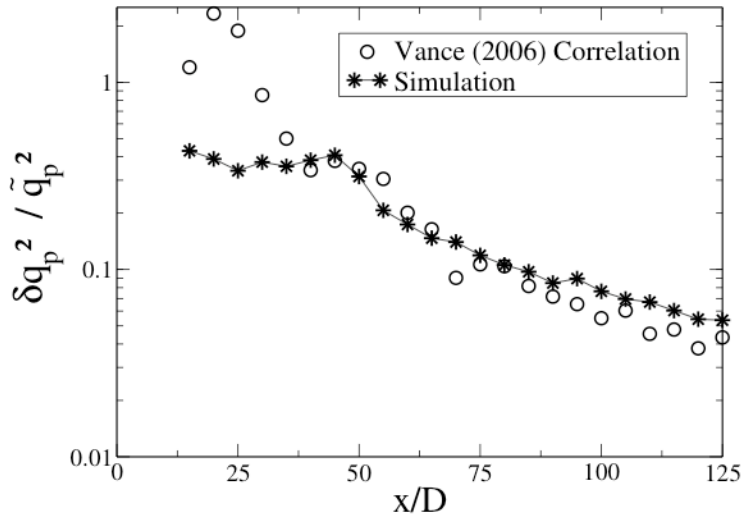

Figure 14: Partitioning of the particle fluctuating motion along axis. Comparison with the correlation of Vance et al. (2006).

$X/D = 40$ in the simulation. This is maybe the consequence of an underestimation of the uncorrelated part on the boundary condition and maybe because

the Vance's correlation has been established from a fully developed turbulent flow. Nevertheless, even if the ratio is not satisfactory near the nozzle exit, it matches very well the correlation after $X/D = 40$ which is closer to the free jet area. The decrease of the uncorrelated energy with the distance to the nozzle exit is very well predicted.

The decomposition of the fluctuating liquid energy into mean correlated, uncorrelated and subgrid is shown radially at $X/D = 100$ on Fig. (15). The subgrid energy q_{SGS} is obtained directly from the expression of the subgrid pressure P_{SGS} defined in Eq. (20) because $q_{SGS} = \frac{P_{SGS}}{\tilde{\alpha}_l \rho_l}$

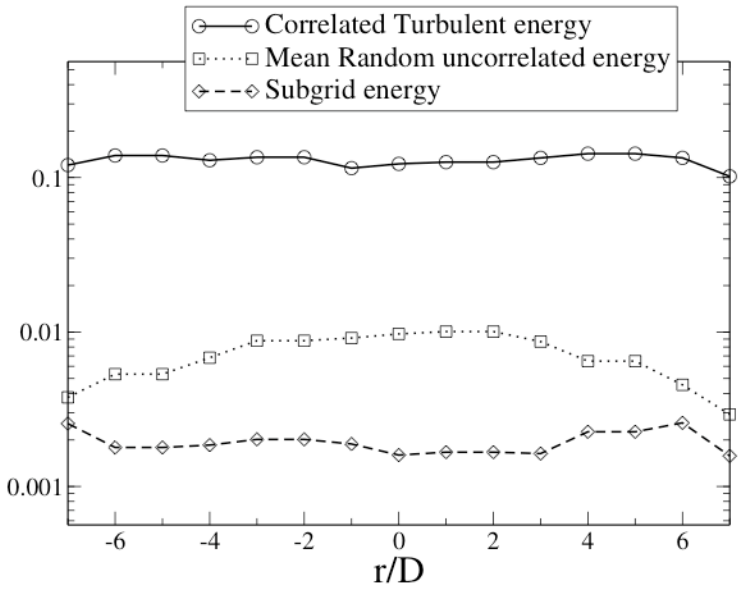

Figure 15: Decomposition of the particle fluctuating motion at 100D. Radial profiles are normalised by the mean correlated energy on spray axis.

All values are normalised by the mean correlated energy on spray axis. The mean uncorrelated energy represents about 10% of the correlated turbulent energy while the subgrid energy is about 2%. According to Pope et al. (2004), the level of subgrid energy compared to the turbulent energy ensures a good quality of the LES.

At the periphery of the spray, the uncorrelated part decreases while the sub-

grid part increases. Their values at $|r/D| = 7$ are almost equal. The decrease of uncorrelated energy shows that the liquid and gas fluctuations are more correlated at the periphery than at the center. Both uncorrelated and subgrid energy are about 0.5% of the mean correlated energy.

5. Concluding remarks

The Large Eddy Simulation (LES) of Diesel Spray using an Eulerian-Eulerian approach has been conducted and compared to the experiment of Chaves et al. (2004). The two-fluid model based on the Mesoscopic Eulerian Formalism is presented with the extension to dense flows by the addition of collision effects. A sensitivity study on boundary conditions parameters has also been treated. In addition, an analysis of the spray dynamics, by comparison with experimental results from literature on turbulent gaseous jets, has been carried out. The following conclusions can be deduced from this work:

- The simulation results show a good tendency compared to the experiment in terms of decrease of axial velocity along axis. Nevertheless, the axial spray velocity is under-estimated in the simulation on the spray axis. In the simulation, the decrease of velocity is comparable to the decrease of velocity in a free turbulent gaseous jet. Our calculation does not take into account the non atomized large droplets that could appear in the experiment and contribute to the high velocity on spray axis. This is confirmed by the radial profile of axial velocity that shows a good concordance at the spray periphery but not at the center. The discrepancy will be less significant under high pressure Diesel injection where atomization is enhanced.

- The calculations are insensitive to the maximum droplet diameter injected or the gas velocity at the boundary conditions. An explanation is that the equilibrium between gas phase and liquid phase is rapidly reached. The most important parameter is the turbulence intensity at injection which

highly influences the spray angle. The level of turbulence can be deduced from the turbulence properties of the gas jet.

- The LES can easily reproduce the impact of the chamber pressure on the spray angle.

- The statistical properties of the gas phase and the liquid phase show a high correlation between them. Futhermore the properties of the liquid phase look similar to those of the turbulent gaseous jet. Self-similarity for the mean axial liquid velocity is reached at a distance of 125 nozzle diameters. The axial velocity decreases like the inverse of the distance to the nozzle exit, corresponding to a linear expansion of the jet with the distance . The self-similarity for the radial fluctuations appear later compared to the axial fluctuations. This proves the anisotropy of the rms fluctuations.

- The liquid volume fraction inside the spray shows instantaneously high local disparities. This segregation could lead to high local differences in the equivalence ratio after evaporation and can strongly impact the combustion and pollutants.

References

Arcoumanis, C., Whitelaw, J., Wong, K., 1989. Gaseous simulations of diesel-type sprays in a motored engine. SAE Paper 890793.

Bellan, J., 2000. Perspectives on large eddy simulations for sprays: issues and solutions. Atomization and Sprays 10, 409–425.

Boelle, A., Balzer, G., Simonin, O., 1995. Second order prediction of the part-phase stress tensor of inelastic spheres in simple shear dense suspensions. In: ASME Gas-Solid Flows Symposium.

Boileau, M., Pascaud, S., Riber, E., Cuenot, B., Gicquel, L., Poinsot, T., Cazalens, M., 2008. Investigation of two fluid methods for Large Eddy Simula-

tion of spray combustion in Gas Turbines. Flow, Turbulence and Combustion 80 (3), 291–321.

Bruneaux, G., 2002. A study of mixture formation in direct injection diesel like conditions using quantitative fuel concentration visualizations in a gaseous fuel jet. SAE SP 2002 Numb 1713, 159–174.

Campbell, C., 1989. The stress tensor for simple shear flows of a granular material. J. Fluid Mech. 203, 449–473.

Chapman, S., Cowling, T., 1939. The Mathematical Theory of Non-Uniform Gases, cambridge mathematical library Edition. Cambridge University Press.

Chaves, H., Kirmse, C., Obermeier, F., 2004. Velocity measurement of dense diesel fuel sprays in dense air. Atomization and Sprays 14, 589–609.

Colin, O., Rudgyard, M., 2000. Development of high-order taylor-galerkin schemes for LES. Journal of Computational Physics 162 (2), 338–371.

Dent, J., 1971. A basis for the comparison of various experimental methods for studying spray penetration. SAE Paper 710571.

Desantes, J., Payri, R., Garcia, J., Salvador, F., 2007. A contribution to the understanding of isothermal diesel spray dynamics. Fuel 86, 1093–1101.

Desantes, J., Payri, R., Salvador, F., Gil, A., 2006. Development and validation of a theoretical model for diesel spray penetration. Fuel 85, 910–917.

Doudou, A., 2005. Turbulent flow study of an isothermal diesel spray injected by a common rail system. Fuel 84, 287–298.

Drake, M., Haworth, D., 2007. Advanced gasoline engine development using optical diagnostic and numerical modeling. Proceedings of the 31^{st} Symposium (Int.) on Combustion, The Combustion Institute.

Fevrier, P., Simonin, O., Squires, K., 2005. Partitioning of particle velocities in gas-solid turbulent flows into a continuous field and a spatially uncorrelated

random distribution: Theoretical formalism and numerical study. J. Fluid Mech. 533, 1–46.

Germano, M., Piomelli, U., Moin, P., Cabot, W., 1991. A dynamic subgrid-scale eddy viscosity model. Physics of Fluids 3 (7), 1760–1765.

Gibson, M., 1963. Spectra of turbulence in a round jet. Journal of Fluid Mechanics 15, 161–173.

Hopkins, M., Louge, M., 1991. Inelastic microstructure in rapid granular flows of smooth disks. Phys. of Fluids 3, 47–57.

Hussein, H., Capp, S., Georges, W., 1994. Velocity measurements in a high-reynolds-number, momentum-conservative, axisymmetriic, turbulent jet. Journal of Fluid Mechanics 258, 31–75.

Iyer, V., Abraham, J., 1997. Penetration and dispersion of transient gas jets and sprays. Combustion. Sci. and Tech. 130, 315–335.

Iyer, V., Abraham, J., 1998. The computed structure of a combusting transient jet under Diesel conditions. SAE technical paper 981071.

Iyer, V., Abraham, J., 2005. Two-fluid modeling of spray penetration and dispersion under diesel engine conditions. Atomization and Sprays 15, 249–269.

Kaufmann, A., 2004. Vers la simulation des grandes chelles en formulation euler-euler des coulements ractifs diphasiques. Ph.D. thesis, Institut National Polytechnique de Toulouse.

Klein, M., Sadiki, A., Janicka, J., 2003. A digital filter based generation of inflow data for spatially developing direct numerical simulation or large eddy simulations. Journal of Computational Physics 186, 652–665.

Kraichnan, R., 1970. Diffusion by a random velocity field. Physics of Fluids 13, 22–31.

Kuo, t.-W., Bracco, F., 1982. On the scaling of transient laminar, turbulent, and spray jets. SAE Paper 820038.

Launder, B., Spalding, D. B., 1972. Mathematical models of turbulence. Academic Press.

Lun, C., Savage, S. B., 1986. The effects of an impact velocity dependent coefficient of restitution on stresses developed by sheared granular materials. Acta Mechanica 63, 15–44.

Martinez, L., Benkenida, A., Cuenot, B., 2009. A model for the injection boundary conditions in the context of 3D simulation of diesel spray: Methodology and analysis. FUEL, in revision.

Moreau, J.-B., 2005. Modélisation de l'écoulement polyphasique à l'intérieur et en sortie des injecteurs Diesel. Ph.D. thesis, Institut National Polytechnique de Toulouse.

Moureau, V., 2004. Simulation aux grandes échelles de l'aérodynamique interne des moteurs á pistons. Ph.D. thesis, Ecole Centrale Paris / IFP Rueil-Malmaison, France.

Naber, J., Siebers, D., 1996. Effects of gas densit and vaporisation on penetration and dispersion of diesel sprays. SAE Paper 960034.

Ouellette, P., Hill, P., 2000. Turbulent transient gas injection. Journal of Fluids Engineering 122, 743–753.

Ozdor, N., Dulger, M., Sher, E., 1994. Cyclic variability in spark ignition engines a literature survey. SAE Technical Paper 940987.

Panchapakesan, N., Lumley, J., 1993. Turbulence. Journal of Fluid Mechanics 246, 197–223.

Payri, R., Tormos, B., Salvador, F., Araneo, L., 2008. Spray droplet velocity characterization for convergent nozzles with three different diameters. Fuel 87, 3176–3182.

Peirano, E., Leckner, B., 1998. Fundamentals of turbulent gas-solid flows applied to circulating fluidized bed combustion. Progress in Energy and Combustion Science 24, 259–296.

Pope, S., Ren, Z., Lu, L., Raman, V., Pitsch, H., 2004. Les/pdf/isat computations of turbulent flames. In: Proc. of the Summer Program. Vol. in press. Center for Turbulence Research, Stanford, USA.

Riber, E., Garcia., M., Moureau, V., Pitsch, H., Simonin, O., Poinsot, T., 2006. Evaluation of numerical strategies for les of two-phase reacting flows. In: Proc of the Summer Program. Center for Turbulence Research, NASA Ames/Stanford Univ., pp. 197–213.

Riber, E., Moreau, M., Simonin, O., Cuenot, B., 2005. Towards large eddy simulation of non-homogeneous particle laden turbulent gas flows using euler-euler approach. In: 11th Workshop on Two-Phase Flow Predictions. Merseburg, Germany.

Richard, S., Colin, O., Vermorel, O., Benkenida, A., Angelberger, C., Veynante, D., 2007. Towards large eddy simulation of combustion in spark ignition engines. Proc. of the Combustion Institute 31 (3059-3066).

Sagaut, P., 1998. Introduction a la simulation des grandes échelles pour les écoulements de fluide incompressible. Mathématiques et Applications, Springer Verlag.

Schiller, L., Nauman, A., 1935. A drag coefficient correlation. VDI Zeitung 77, 318–320.

Schmitt, P., Poinsot, T., Schuermans, B., Geigle, K., 2007. Large-eddy simulation and experimental study of heat transfer, nitric oxide emissions and combustion instability in a swirled turbulent high pressure burner. J. Fluid Mechanics 570, 17–46.

Selle, L., Benoit, L., Poinsot, T., Nicoud, F., Krebs, W., 2006. Joint use of compressible large-eddy simulation and helmoltz solvers for the analysis of

rotating modes in an industrial swirled burner. Combust. Flame 145 (1-2), 194–205.

Simonin, O., Fevrier, P., Lavieville, J., 2002. On the spatial distribution of heavy particle velocities in turbulent flow : from continuous field to particulate chaos. Journal of Turbulence 3.

Smirnov, A., Shi, S., Celik, I., 2001. Random flow generation technique for large eddy simulations and particle-dynamics modeling. Trans. ASME. Journal of Fluids Engineering 123, 359–371.

Spalding, D. B., 1979. Combustion and mass transfer. No. ISBN 0-08-022105-8. Pergamon Press.

Truchot, B. B. A., Magnaudet, J., 2005. Modelling of turbulence in the context of an eulerian approach for simulating two-phase flow in internal combustion engines. In: 20th Annual ILASS Meeting.

Vance, M., Squires, K., Simonin, O., 2006. Properties of the particle velocity field in gas-solid turbulent channel flow. Physics of Fluids 18, 063302.

Vermorel, O., Richard, S., Colin, O., Angelberger, C., Benkenida, A., 2007. Multi-cycle LES simulations of flow and combustion in a PFI SI 4-valve production engine. SAE PAPER 2007-01-0151.

Wu, K.-J., Santavica, D., Bracco, F., Coghe, A., 1984. A ldv measurements of drop velocity in diesel-type sprays,. AIAA Journal 22 (9), 1263–1270.

Wygnansky, I., Fielder, H., 1969. Some measurements in the self-preserving jet. Journal of Fluid Mechanics 38, 577–612.